PLOS ONE

A proposed population-health based metric for evaluating representativeness of air quality monitoring in cities: Using Hong Kong as a demonstration

Tilman Leo Hohenberger[1], **Wenwei Che**[1]*, **Jimmy C. H. Fung**[1,2], **Alexis K. H. Lau**[1,3,4]

1 Division of Environment and Sustainability, The Hong Kong University of Science and Technology, Clear Water Bay, Hong Kong, China, **2** Department of Mathematics, The Hong Kong University of Science & Technology, Clear Water Bay, Hong Kong, China, **3** Department of Civil and Environmental Engineering, The Hong Kong University of Science and Technology, Clear Water Bay, Hong Kong, China, **4** Institute for the Environment, The Hong Kong University of Science & Technology, Clear Water Bay, Hong Kong, China

* wenweiche@ust.hk

Abstract

City air quality monitoring (AQM) network are typically sparsely distributed due to high operation costs. It is of the question of how well it can reflect public health risks to air pollution given the diversity and heterogeneity in pollution, and spatial variations in population density. Combing high-resolution air quality model, spatial population distribution and health risk factors, we proposed a population-health based metric for AQM representativeness. This metric was demonstrated in Hong Kong using hourly modelling data of PM_{10}, $PM_{2.5}$, NO_2 and O_3 in 2019 with grid cells of 45m * 48m. Individual and total hospital admission risks (%AR) of these pollutants were calculated for each cell, and compared with those calculated at 16 monitoring sites using the similarity frequency (SF) method. AQM Representativeness was evaluated by SF and a population-health based network representation index (PHNI), which is population-weighted SF over the study-domain. The representativeness varies substantially among sites as well as between population- and area-based evaluation methods, reflecting heterogeneity in pollution and population. The current AQM network reflects population health risks well for PM_{10} (PHNI = 0.87) and $PM_{2.5}$ (PHNI = 0.82), but is less able to represent risks for NO_2 (PHNI = 0.59) and O_3 (PHNI = 0.78). Strong seasonal variability in PHNI was found for PM, increasing by >11% during autumn and winter compared to summer due to regional transport. NO_2 is better represented in urban than rural, reflecting the heterogeneity of urban traffic pollution. Combined health risk ($\%AR_{total}$) is well represented by the current AQM network (PHNI = 1), which is more homogenous due to the dominance and anti-correlation of NO_2 and O_3 related %AR. The proposed PHNI metric is useful to compare the health risk representativeness of AQM for individual and multiple pollutants and can be used to compare the effectiveness of AQM across cities.

of 45m * 48m. To facilitate people to verify our methods, we have generated a sample dataset (with 30 random days of pollution data in the same temporal and spatial resolution as we used in the paper), which is publicly available at http://envf.ust.hk/dataview/aqms_rep/current/ after filling a simple questionnaire. For further use of the PRAISE-HK generated data, we encourage interested researchers to contact IENV (webenvf@ust.hk) with their purpose of use and dataset need to discuss the online sharing of the data. Detailed data can be extracted and shared case by case in a collaborative manner to encourage productive downstream uses.

Introduction

Urban air-pollution is a severe driver of mortality and loss of disability-adjusted life years (DALY), and associated with a number of short -and long-term health complications such as respiratory diseases [1], pulmonary diseases [2], cancer [3] or heart diseases [4]. Globally, more than 80% of city-dwellers experience air quality levels that exceed the World Health Organization's (WHO's) limits [5]. Dominant air pollutants include particulate matter of various sizes (generally classified as PM_{10} with a diameter of < 10 micrometres, and $PM_{2.5}$ with a diameter of < 2.5 micrometre), as well as gaseous pollutants as Nitrogen Dioxide (NO_2) and Ozone (O_3) [6, 7].

In many cities, air quality measured from fixed-site monitoring (FSM) stations is typically used for public information and regulatory compliance [8]. Due to high expense and complexity in operation, the distribution of FSM is typically sparse in space, e.g. district-based [9]. However, due to complexities in weather, emission and urban morphology, urban air quality exhibit high spatial and temporal variability [10]. Knowing how well FSM can reflect variations in air quality becomes important for epidemiological studies, compliance to regulation, decision making of individual citizens and while setting up, moving or removing obsolete sensors in a network.

Many approaches have been developed to evaluate the representativeness of FSM, including simple geometry [11], classification by land use [12, 13], remote sensing [14], chemical transportation models [15, 16], computational fluid dynamics [17] or classification based on environmental parameters [18]. In recent years, high-resolution air quality data down to street level become available with the development of urban air quality models. For example, Rodriguez *et al.* used the Parallel Micro-Swift-Spray (PMSS) to evaluate the representativeness of FSM, which achieved a resolution of 3 metres [19]. However, this and the previous methods are mostly developed to evaluate spatial representation [20] as well as the ability to detect standard violations [21]. There is a lack of consideration of health impacts, which is the primary goal in formulating air quality guidelines and control strategies. A paradigm of health-based evaluation is needed to judge and compare the representativeness of FSMs to deliver proper information for public health.

The health risk of air pollution at a certain place depends on the abundance of different air pollutants measured or estimated at that location and the toxicity of air pollutants. Concentrations reported by FSM may reflect the abundance of different air pollutants. Still, these concentrations cannot be added or compared among pollutants for health risk because of differences in toxicity. For example, the added short-term health risk in hospital admission is a 0.51% per unit increase in O_3 concentration (10 μg/m³) while it is a 0.28% per unit increase in PM_{10} concentration (10 μg/m³) in Hong Kong [22]. To deliver health risks information from total air pollution, Stieb *et al.* proposed an air quality health index (AQHI) which transformed the air pollutants concentrations at a given location into additive health risks [23]. The resulting added health-risks (%AR_{total}) from the AQHI method can be used to express total health risks of air pollution at a given location as well as contributions to it from different pollutants, which can be a useful metric in evaluating the representatives of FSMs for health risks.

Total health impacts of an urban population do not only depend on the geographical variability in health risks calculated by %AR, but also on the population distribution. In a single city, people live in places with substantial variability in air quality. In epidemiological studies, areas with higher population density would be granted heavier weights when estimating the total health impacts for the whole population [24, 25]. Modern cities, such as Hong Kong are very heterogeneous in population distribution, which may lead to substantial differences in total health risk estimates among FSMs compared to traditionally used space-based method.

This is especially important when evaluating whether an FSM should be set up, moved or removed from a monitoring network regarding the public health for the whole community.

In the light of the increasing importance of inter-city competition [26, 27], city-networks [28], urbanisation [29], and fast-changing pollution levels [30, 31], a comparable metric to judge the quality of air-pollution management would enormously benefit accountability and good-governance efforts. As urban areas around the globe are facing locally different air-pollution challenges and individual pollutants contribution to total health impacts can vary, such a metric should be based on the representation of public health impacts from air-pollution derived of local risk factors, and not on the representation of individual pollutant species' concentration levels.

Following these considerations, this study proposes a population-health risk-based method in evaluating the representativeness of urban FSM networks, which is able to: (1) assess and compare the representativeness of health risks among FSMs for different pollutants (including PM_{10}, $PM_{2.5}$, NO_2, and O_3) and for total short term health impacts ($\%AR_{total}$); (2) evaluate the representativeness of whole air quality monitoring network for single and combined health risks of pollutants.

The method will be demonstrated using Hong Kong as a testbed. There are sixteen FSMs spatially distributed over an area of 1,100 km^2 in Hong Kong, located in areas of different functionalities such as roadside, residential, commercial, industrial urban areas, and rural areas. The accessibility of air quality monitoring data from these stations provides a unique opportunity to investigate the representativeness of FSMs regarding heterogeneity in their geographic location and function.

Materials and methods

This section includes: (1) study area and FSMs that would be assessed in this study; (2) a description of high-resolution air quality models, which provide fine-scale air quality data to compare with the air quality reported by FSM; (3) heath-risk based evaluation method for FSM representativeness evaluation; and (4) population-health based network index.

Study area and FSMs

Hong Kong is selected to demonstrate the proposed metrics due to its heterogeneity in geographical features, population density and land-use, which are common in modern cities.

Hong Kong's territory is located at the south-eastern tip of China and encompasses 1111 km^2 of land [32]. The territory can be divided into Hong Kong Island, which on a small slip on its northern coastline is highly urbanized, the highly developed Kowloon Peninsula and the relatively rural New Territories. Densely developed "*New-Towns*" are often central to the commercial and residential life in the New Territories. Due to legislation, only 7% of Hong Kong territory is used for human settlements [32], which makes Hong Kong one of the world's most densely populated cities. The total population accounts for roughly 7.5 million people [33]. Fig 1 displays the population-distribution in Hong Kong.

Outdoor air pollution has significant seasonal variations in Hong Kong due to the Asian monsoon system (Table 1). The persistent northeast monsoon in winter brings pollution from the Asian continent, whereas the summer monsoon shifts to south-westerly winds that bring in cleaner marine air [34].

The Hong Kong Environmental Protection Department (HKEPD) runs an FSM network comprising of 12 general stations, three roadside stations and one background station. Locations of FSM stations are shown in Fig 1. Hourly data of PM_{10}, $PM_{2.5}$, NO_2 and O_3 were obtained from HKEPD for 2019.
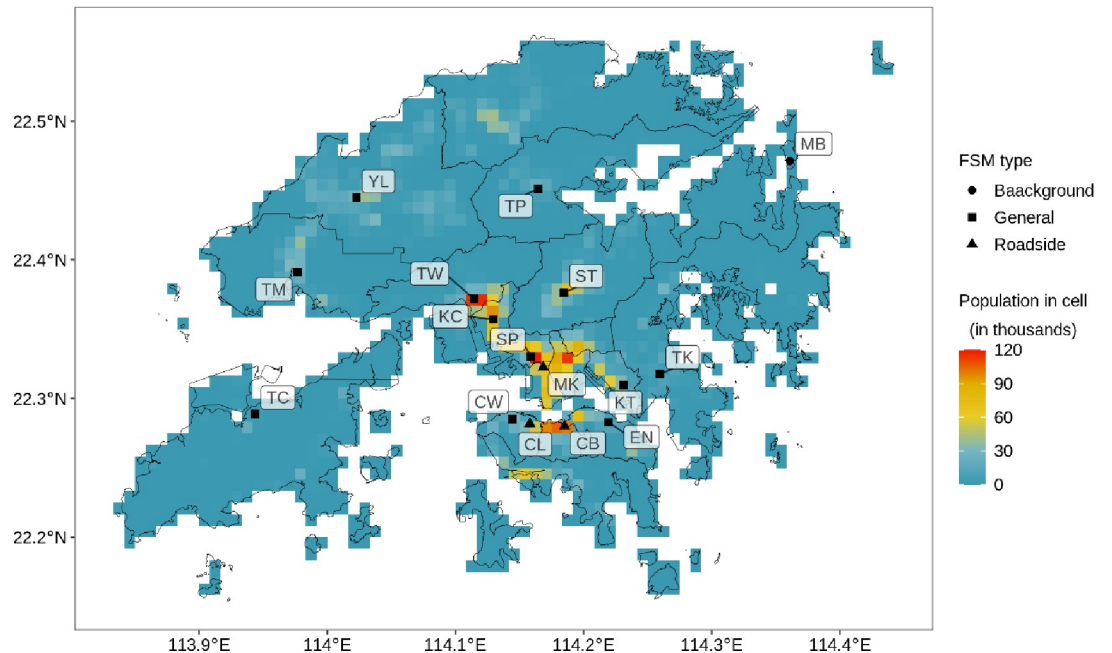
Fig 1. Population density and fixed site monitor (FSM) locations in Hong Kong's districts, with FSM abbreviated as: Causeway Bay (CB), Central (CL), Central Western (CW). Eastern (EN), Kwai Chung (KC), Kwun Tong (KT), Tap Mun (MB), Mong Kok (MK), Sham Shui Po (SP), Sha Tin (ST), Tung Chung (TC), Tseung Kwan O (TK), Tuen Mun (TM), Tai Po (TP), Tsuen Wan (TW), Yuen Long (YL). Outlines of Hong Kong's districts reprinted from Esri China (Hong Kong) under a CC BY license, with permission from Esri China (Hong Kong), original copyright 2017.

General stations are located on rooftops of public infrastructure such as commu-nity buildings, or libraries with a height between 13 to 28 metres [35]. The degree of urbaniza-tion of surrounding areas varies strongly between stations. However, general stations are typically located in centres of or urban districts and "*New-Towns*" (Fig 1). In contrast, the three roadside stations are located next to busy roads, with inlets on a level of around 3 to 4.5 metres. All three roadside stations are concentrated in the highly developed part of the terri-tory. The background station is located on a small and undeveloped island at Hong Kong's north-east at 11 metre height. It reflects the background concentration that was transported into Hong Kong in winter due to its upwind location.

High resolution air quality models

This study takes advantage of a coupled regional and urban modelling system to provide fine-scale air quality data down to street-level. The modelling system consists of a regional model, Community Multiscale Air Quality Modelling System (CMAQ) [36], coupled with an urban transport model, Atmospheric Dispersion Modelling System in the urban area (ADMS-urban) [37].

Table 1. Annual and seasonal means over all general FSM stations for selected air pollutants.

	Unit	Annual	Spring	Summer	Autumn	Winter
PM$_{10}$	µg/m^3	32.2	26.7	20.9	40.7	40.6
PM$_{2.5}$	µg/m^3	19.2	16.5	12.1	23.9	24.4
NO$_2$	ppb	20.5	19.1	16.8	21.0	25.0
O$_3$	ppb	30.4	29.7	21.1	44.8	26.0

CMAQ takes inputs from a numerical weather prediction model, Weather Research and Forecasting model (WRF) [38], and a regional emissions model, Sparse Matrix Operator Kernel Emissions (SMOKE) [39], and by taking account of both chemical and physical conversions, produces a regional pollution forecast for nested domains at multiple grid spatial resolution down to 1 km by 1 km. ADMS-Urban then adds spatial resolution for the study area (Hong Kong's territory) and produces hourly pollution values on a dynamic grid of down to 2-metre resolution by including localized sources (e.g. road-emissions) and urban morphology. A detailed description of the coupled system is available from Che *et al* [10].

Model verification was conducted by comparing model outputs against observational data from FSMs on an hourly basis for the year of 2019. Here, the ADMS-Urban output point closest to an FSM was compared to the actual FSM readings. Following past papers, we used the Index of Agreement (IOA) and Root Mean Square Error (RMSE) as the necessary model verification [10, 13, 40]. Formulas for IOA and RMSE are given in Eqs 1 and 2 [41].

Eq 1: IOA formula

$$IOA = 1 - \frac{\sum_{i=1}^{N}(P_i - O_i)^2}{\sum_{i=1}^{N}(P_i + -O + O_i - -O)^2} \tag{1}$$

Eq 2: RMSE formula

$$RMSE = \sqrt{\frac{\sum_{i=1}^{N}(P_i - O_i)^2}{N}} \tag{2}$$

, where P are predicted (modelled) values and O are observed values.

IOA is used to evaluate to which extent the deviations of hourly observations averaged over all hours corresponds to the deviations of hourly model predictions averaged over all hours [10]. A detailed discussion on IOA as a metric for air-pollution models is available from Kang *et al.* [42].

ADMS-Urban produces a dynamic mesh of output points, with a higher resolution in proximity to pollution sources (roads, industrial sources, etc). To be able to compare areas with a different number of output points and at the same time maintaining a high spatial resolution, we divided Hong Kong's territory into 1000000 raster cells of each ~3000m^2 (45 x 48 metres). For every timestep, the concentration-value of a raster cell was set to the arithmetic mean of the concentrations of all ADMS output points inside the respective raster cell. Fig 2 depicts the rasterization of ADMS output points, while at the same time showing the clustering of output points around road sources. The rasterization of the dynamic mesh was achieved using Eq 3.

Eq 3: Calculation of arithmetic means for all raster cells from model output points

$$\forall i \in \{1, \ldots, n\}. \, rc_{p,i,t} = \frac{\sum_{j=1}^{k_i} mc_{p,j,t}}{k_i} \tag{3}$$

where, n is the number of raster cells, rc is the concentration of raster cell for pollutant p at timestamp t, mc is the model output concentration at model output point j, and k is the number of model output points located in cell i.

Further, using a simple intersection between the raster grid and each FSM location, we derived the corresponding raster cell for each FSM station. The pollutant concentrations (after
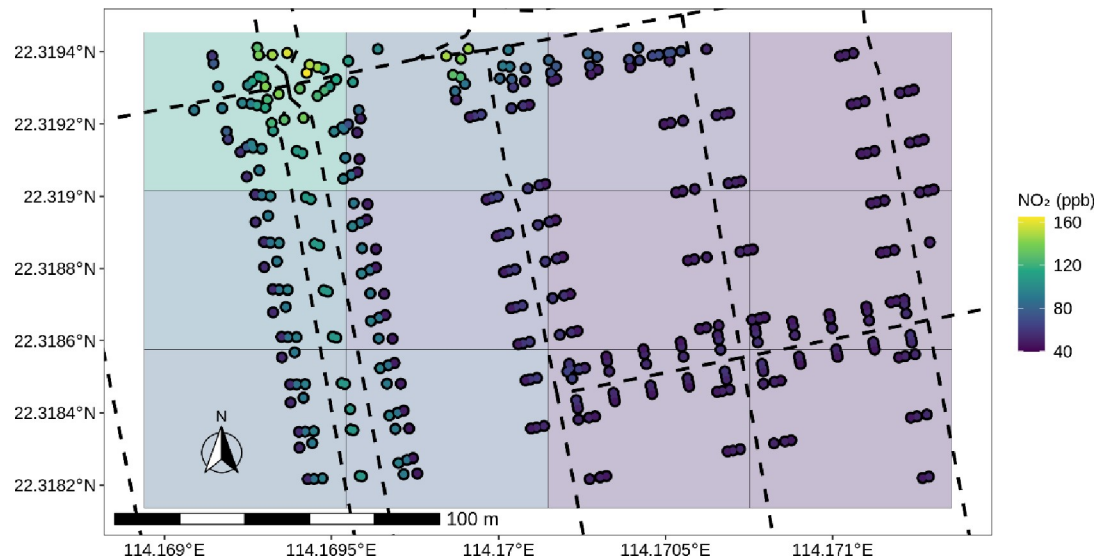
Fig 2. Conversion from dynamic mesh of ADMS model output (points) to raster, with streets (dashed lines).

Eq 3) of this corresponding raster cell was set as a "pseudo-station" [19] for each FSM. The representativeness calculation is based on the correlation of these "pseudo-stations" with all other raster cells.

Health-risk based representativeness evaluation approach

This study introduces the additive health risk approach [23] in developing the metrics for FSM representativeness evaluation, and used local health risks coefficients to calculate the %AR. These coefficients were derived by Wong *et al.* [22, 43] based on the relationship between hospital admissions and measured pollution concentrations in Hong Kong. The hospital admission risks for all age-groups increase 0.022%, 0.028%, 0.045% and 0.051% for every $10\mu g/m^3$ increase in concentrations of $PM_{2.5}$, PM_{10}, NO_2, and O_3, respectively. These values were used to evaluate the short-term health risks from air pollutants. The long-term health risk is not considered in this study due to a lack of proper health coefficients.

The %AR was calculated for the simulated air pollutants from CMAQ/ADMS models using Eq 4.

Eq 4: Additional health risk (%AR)

$$\%AR_{p,j,t} \; = \; \left(e^{(\beta_p \times C_{p,j,t})} - 1\right) x \; 100\% \tag{4}$$

Where,

$\%AR_{p,j,t}$ = added health-risks in the hospitalization of pollutant p in cell j at timestamp t (unitless);

$C_{p,j,t}$ = the modelled pollutant concentration (in $\mu g/m^3$);

β_p = Hospital admission increase rates for pollutant p.

A major upside of an %AR based index is its ability to aggregate the health risks of different air-pollutants. The total $\%AR_{total}$ expresses the combined short-term hospitalisation risk from multiple pollutants in a given area (Eq 5).

Eq 5: Total additional health risk (%AR_{total})

$$\%AR_{total,j,t} = \%AR_{NO_2,j,t} + \%AR_{O_3,j,t} + \max\{\%AR_{PM_{2.5},j,t} + \%AR_{PM_{10},j,t}\} \tag{5}$$

Additional health risk of PM takes %AR from either $PM_{2.5}$ or PM_{10}, whichever is higher on a given time-step and location (27).

Subsequently, the similarity frequency (SF) method [44] was applied to %AR values (%AR_{total}, as well as individual pollutants) as the basis to calculate health-based representativeness areas. SF aims at calculating the ratio at which a pollutant concentration (may it be measured or modelled) at point A does not differ more than X percent from a pollutant concentration at point B. The methodology of SF has been described before in greater detail [15, 16]. In this work, it is used to compare the similarity in %AR between modelled pollutants at raster cells and modelled pollutants at pseudo-stations. We follow the convention of setting the threshold value for similarity as 20% difference in %AR [13, 19, 44]. SF then equals to the ratio of timesteps that satisfy the similarity criterion against the number of total timesteps. The SF scale ranges from 0 (no representation) to 1 (high representation). A SF > 0.9 shows good representation [44]. We divided the SF scale into further bands, with < 0.5 deemed as low representation, $0.5 < SF < 0.7$ as medium representation, $0.7 < SF < 0.9$ as medium to high, and SF > 0.9 as high representation. The representativeness of individual FSM was assessed by adding up the total area and population of cells with SF > 0.9.

In the following, Eq 6 was used to derive each cell's representativeness by the FSM network. For a given cell, the %AR-based SF is calculated between the cell and all pseudo-stations, and the highest value is taken as its representativeness by the FSM network.

Eq 6: Representativeness of a cell by the FSM network

$$\forall i \in \{PS\}.\ R_{p,j} = max\{SF_{\%AR_{p,j}\ \%AR_{p,i}}\} \tag{6}$$

Where,

$R_{p,j}$ = health-based representation at raster cell j;

p = pollutant of pollutant-set, or total pollutants aggregated under Eq 5;

PS = cells in which FSM are located (*pseudo-stations*)

$SF_{\%AR_{p,j}\ \%AR_{p,i}}$ = SF of %$AR_{p,j}$ (raster-cell) and %$AR_{p,i}$ (*pseudo-station*)

Population-health network representation index (PHNI)

We defined the representativeness of the FSM network for a given pollutant, or for the sum of the total short-term health effects of all pollutants (%AR_{total}), as the population-weighted health-based representativeness of the target domain, averaged by the total population in the target domain. Eq 7 shows the calculation of the population-health network representation index (PHNI).

The spatial distribution of Hong Kong's population density was derived from the LandScan dataset [45] with a spatial resolution of 1 km x 1 km, following Lin et al. [46]. The summed population over the study domain is 7.1 million, which is equivalent to the total population of Hong Kong in 2011 [47]. The nearest neighbour algorithm was used to resample the resolution of the LandScan dataset to the resolution of the pollution raster [48]. The target domain can be set to areas of interest, may it be the complete urban territory, or smaller units inside a city (e.g. inner-city administrative boundaries). In the following, we calculated the PHNI for the

whole of Hong Kong, as well as for each of the city's 18 districts, in order to enable relevant inter- and intra-city comparisons.

Seasonal (Summer: June–August, Autumn: September–November, Winter: December–February, Spring: March–May) and annual network indices have been calculated for the year of 2019.

Eq 7: Population-health network representation index

$$\text{PHNI}_{p,d} = \frac{\sum_{i=1}^{n_d} R_{p,i} \times pop_i}{\sum_{i=1}^{n} pop_i} \tag{7}$$

Where, $\text{PHNI}_{p,d}$ is the population-health based network representation index for pollutant p in domain d, n_d is the number of cells in the target domain d, $R_{p,i}$ is the health-based representation of cell i for pollutant p and pop_i is the population count of cell i.

Results

The results include model verification summary, area- and population- based representativeness for aggregated health risks and each selected pollutant, and the annual and seasonal population-health based network indices. We further show the population-health based representation of Hong Kong on the district level.

CMAQ/ADMS model verification

The coupled CMAQ-ADMS-Urban model performed best at predicting particulates, with an average IOA of 0.7 for $PM_{2.5}$ and of 0.72 for PM_{10} between all stations, based on annual hourly model results and concentration readings (Table 2). The highest IOA was found at TM, a

Table 2. Model result verification based on hourly values of the year 2019 for all FSM stations to their respective pseudo-station (raster-cell) for station-types (B = background, R = roadside, G = general).

Station ID	Station Type	PM_{10}		$PM_{2.5}$		NO_2		O_3	
		RMSE (μg/m³)	IOA	RMSE (μg/m³)	IOA	RMSE (ppb)	IOA	RMSE (ppb)	IOA
MB	B	16.5	0.74	11.5	0.75	9.1	0.46	0.6	0.54
CB	R	24.2	0.66	17.8	0.66	23.6	0.67	0.3	0.32
CL	R	21.4	0.67	15.5	0.69	26.9	0.58	0.3	0.36
MK	R	20.1	0.74	18.0	0.67	41.2	0.53	0.4	0.52
CW	G	18.9	0.74	16.2	0.70	33.1	0.43	0.5	0.65
EN	G	18.2	0.74	16.6	0.66	37.7	0.37	0.5	0.64
KC	G	16.0	0.74	13.9	0.70	31.9	0.53	0.5	0.57
KT	G	21.0	0.69	13.9	0.72	22.1	0.63	0.5	0.55
ST	G	17.2	0.71	15.9	0.63	44.0	0.36	0.4	0.64
SP	G	18.5	0.73	16.2	0.64	33.8	0.50	0.5	0.60
TP	G	19.0	0.72	14.8	0.72	15.8	0.61	0.5	0.53
TK	G	15.8	0.75	12.4	0.75	16.8	0.63	0.5	0.57
TW	G	18.3	0.72	15.2	0.71	34.8	0.47	0.5	0.57
TM	G	25.5	0.69	16.1	0.74	21.8	0.63	0.5	0.56
TC	G	20.4	0.68	15.0	0.71	27.1	0.51	0.4	0.58
YL	G	23.2	0.72	15.9	0.70	18.8	0.67	0.5	0.53
Average		19.6	0.72	15.3	0.70	27.4	0.54	0.5	0.55

https://doi.org/10.1371/journal.pone.0252290.t002

background site close to the neighbouring mainland city of Shenzhen, indicating regional impact on particulates.

The model performed less well for gaseous pollutants (IOA averaged between all stations NO_2: 0.54; O_3: 0.55). For NO_2, the model performed better at roadside stations (mean = 0.59) than general stations (mean = 0.53), indicating the influence of the traffic emission on urban NO_2 concentrations. For O_3, the model performed better at general stations (mean = 0.58), and less well at roadside stations (mean = 0.40). This is partly due to the complex interplay of NO_x and VOCs concentrations [49] and sunshine [50] acting on O_3 concentrations at the roadside.

Spatial map of health risk representativeness

Following our outlined approach, annual and seasonal health-risk representativeness maps for Hong Kong's territory were generated for %AR of PM_{10}, $PM_{2.5}$, NO_2, O_3, and combined health risks (%AR_{total}).

The current FSM network represents health risks for PM well. Most of the inhabited areas are represented with a SF > 0.9 for PM_{10} (Fig 3) and SF > 0.7 for $PM_{2.5}$ (Fig 4). In Hong Kong, PM concentrations are greatly influenced by regional and super-regional transport [34, 51], accounting for 60–70% of PM_{10} mass [52], and around 40% of $PM_{2.5}$ mass [34]. The good results of PM %AR representation are partially because of the concentration homogeneity resulting from predominantly regional sources, especially for PM_{10}. The SF values were stronger in Autumn and Winter due to the enhancement of the regional contribution to PM [52], which leads to elevated concentrations in these two seasons as seen in Table 1. The aggregated areas that were well represented (SF > 0.9) for PM vary substantially among sites. Larger well-represented areas were observed at general stations for PM_{10} (mean = 9.22 km^2) compared to $PM_{2.5}$ (mean = 4.00 km^2) than those at road site (PM_{10}: mean = 0.99 km^2; and $PM_{2.5}$: mean = 0.63 km^2). The sampling inlets for general stations are set well above the ground (13 to 28 metres), which makes them more useful to indicate area-wide air quality, where the sampling heights at the roadside are prone to ground emission (3 to 4.5 meters). The largest well-represented area for PM_{10} (88.39 km^2) and $PM_{2.5}$ (96.25 km^2) was found at MB, a background site indicating regional pollution.

The representativeness for health risks related to NO_2 strongly follows the patterns of urban development, leaving many rural areas underrepresented (Fig 5). There are only 13.4 km^2 of Hong Kong's total area is well-represented (SF > 0.9), which are limited to the proximity of stations. This reflects the heterogeneity of NO_2 pollution which are closely related to urban morphology and local traffic emissions as seen from the inset of Fig 5. For example, clear distinctions in SF values are observed between urban and rural areas in Hong Kong Island. High SF values are concentrated on Nathan road, where a roadside monitor is located with heavy-traffic loads. In rural areas and country parks, the SF values are often lower than 0.3. An exception is the background station, which has approximately 4 km^2 well-represented (SF > 0.9) areas. This station is surrounded by a large uninhabited area which is less affected by urban morphology and traffic emissions. The spatial representation of %AR NO_2 patterns are similar throughout the seasons, with slightly higher representation during winter months related to regional pollution.

Most land areas are represented with a SF higher than 0.7 for O_3 (Fig 6). Compared to NO_2, there are large rural areas well-represented (SF > 0.9) for health risks related to O_3 by the current network. For example, the TC station, which is located in a largely undeveloped area, is able to well represent over 20 km^2 of %AR O_3. In contrast, the representativeness in some of the developed urban area is poor. For example, the heavily built-up eastern Kowloon peninsula

(a) Annual representativeness for Hong Kong (left) and its inset area (right)

(b) Spring

(c) Summer

(d) Autumn

(e) Winter

Fig 3. Representativeness of hospital admission risks (%AR) from fixed site monitor (FSM) network over Hong Kong based on annual and seasonal PM$_{10}$ concentrations in 2019. Outlines of Hong Kong's districts reprinted from Esri China (Hong Kong) under a CC BY license, with permission from Esri China (Hong Kong), original copyright 2017.

https://doi.org/10.1371/journal.pone.0252290.g003

(a) Annual representativeness for Hong Kong (left) and its inset area (right)
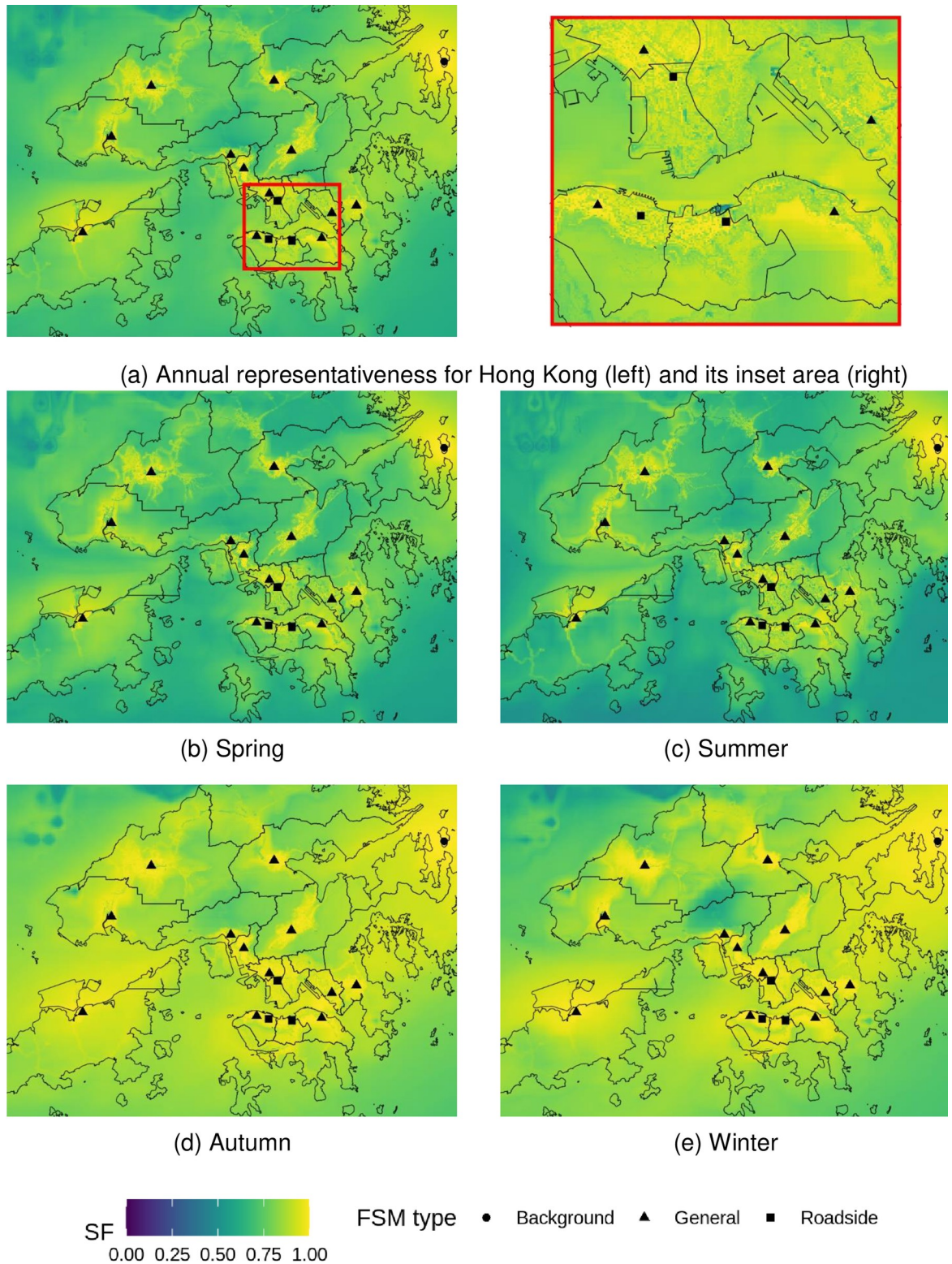
(b) Spring

(c) Summer

(d) Autumn

(e) Winter

Fig 4. Representativeness of hospital admission risks (%AR) from fixed site monitor (FSM) network over Hong Kong based on annual and seasonal PM$_{2.5}$ concentrations in 2019. Outlines of Hong Kong's districts reprinted from Esri China (Hong Kong) under a CC BY license, with permission from Esri China (Hong Kong), original copyright 2017.

https://doi.org/10.1371/journal.pone.0252290.g004

(a) Annual representativeness for Hong Kong (left) and its inset area (right)

(b) Spring

(c) Summer

(d) Autumn

(e) Winter

Fig 5. Representativeness of hospital admission risks (%AR) from fixed site monitor (FSM) network over Hong Kong based on annual and seasonal NO₂ concentrations in 2019. Outlines of Hong Kong's districts reprinted from Esri China (Hong Kong) under a CC BY license, with permission from Esri China (Hong Kong), original copyright 2017.
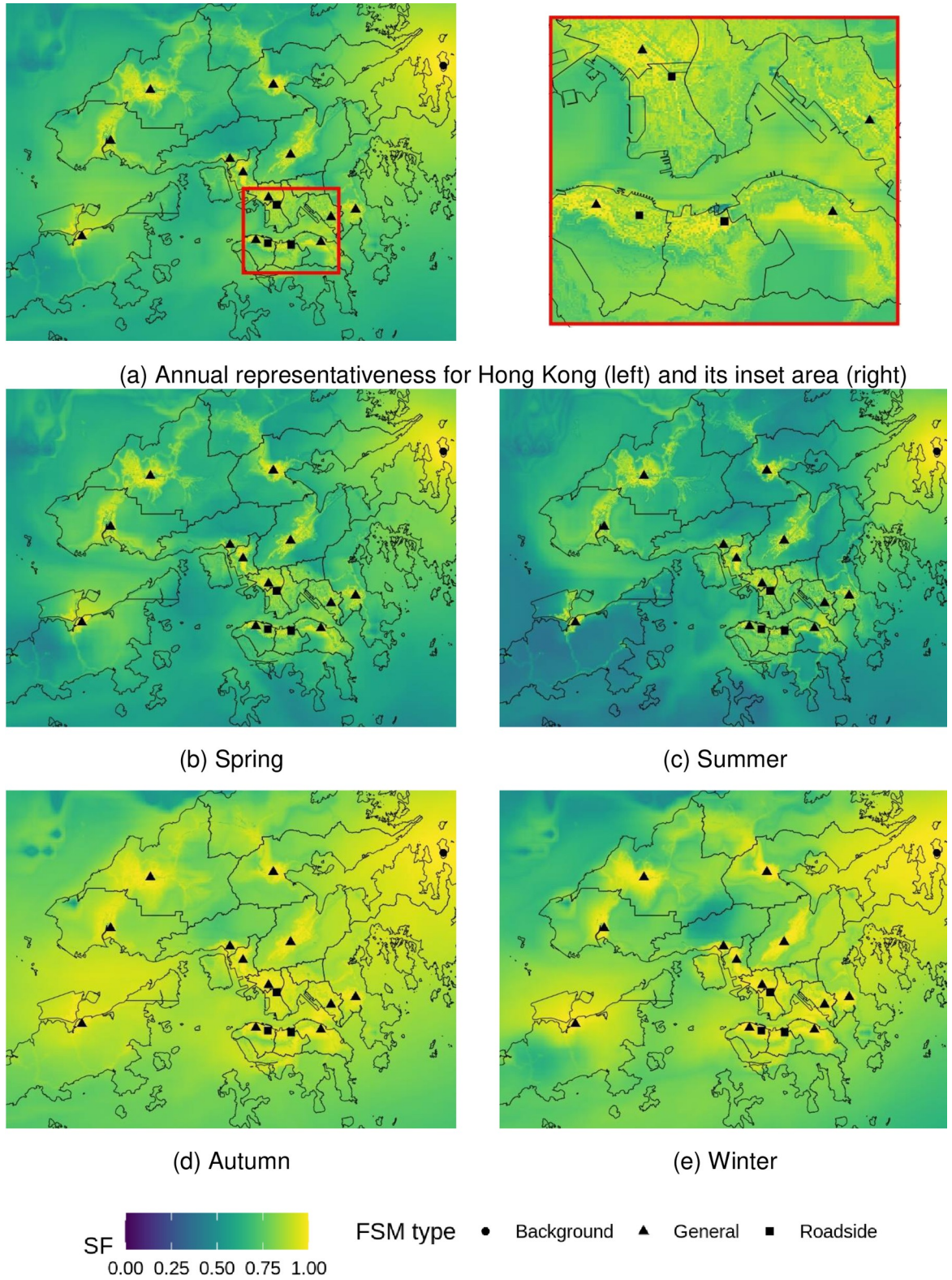
https://doi.org/10.1371/journal.pone.0252290.g005

(a) Annual representativeness for Hong Kong (left) and its inset area (right)

(b) Spring

(c) Summer

(d) Autumn

(e) Winter

Fig 6. Representativeness of hospital admission risks (%AR) from fixed site monitor (FSM) network over Hong Kong based on annual and seasonal O_3 concentrations in 2019. Outlines of Hong Kong's districts reprinted from Esri China (Hong Kong) under a CC BY license, with permission from Esri China (Hong Kong), original copyright 2017.
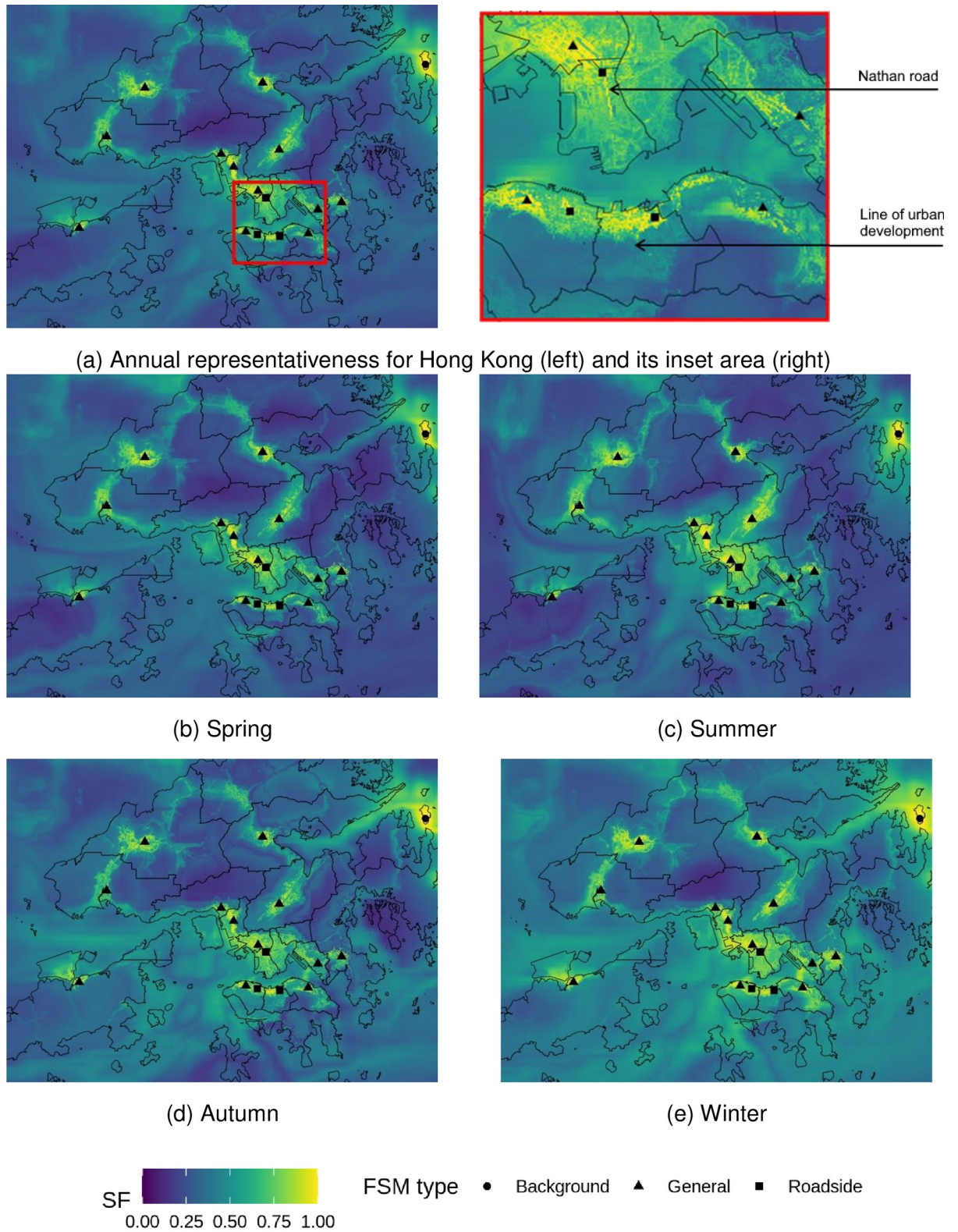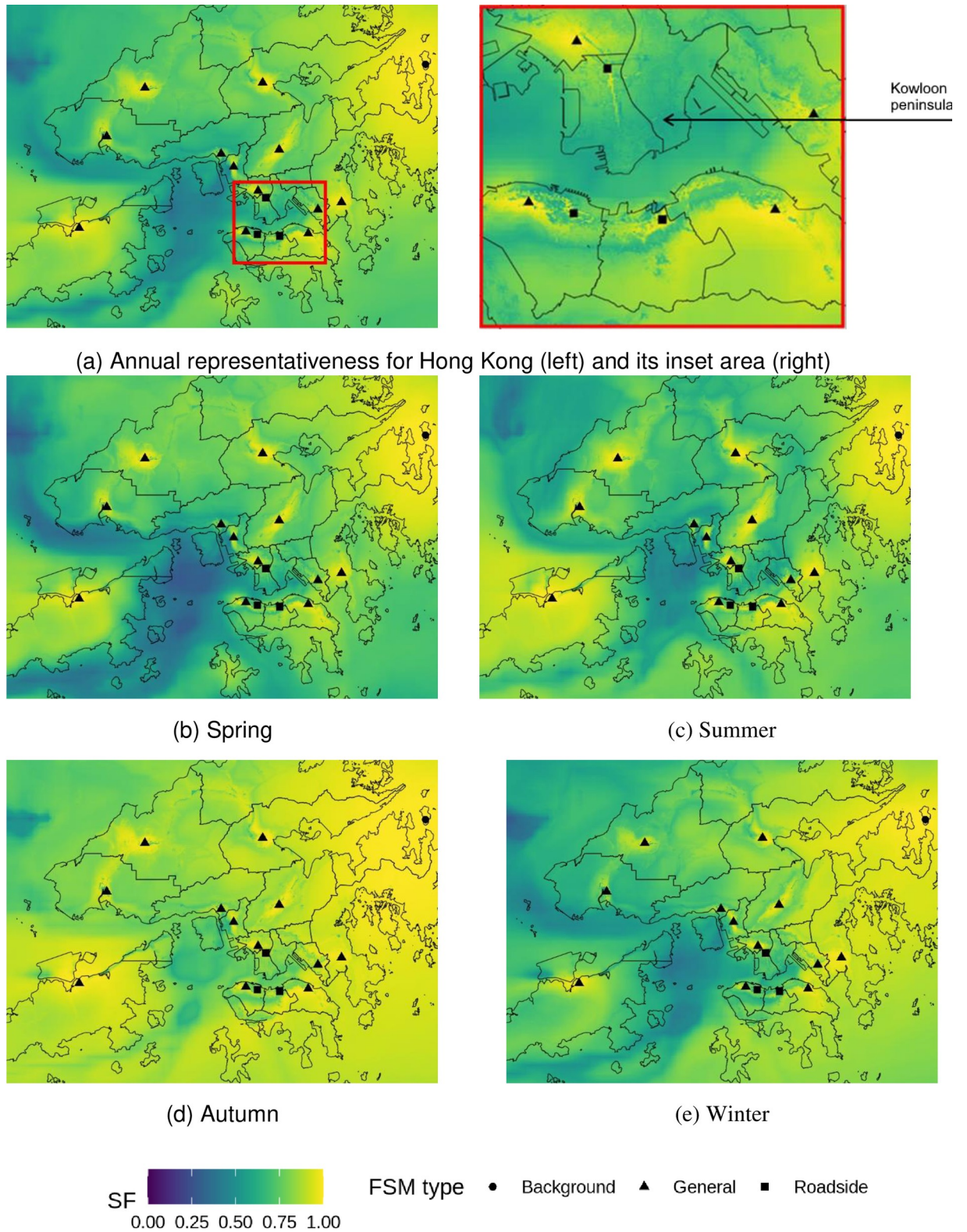
https://doi.org/10.1371/journal.pone.0252290.g006

is notably less represented with most SF values smaller than 0.5. Roadside stations contribute little to the spatial representation of O_3 (mean = 0.19 km^2 of the area represented with SF > 0.9), which is related to the high heterogeneity in NO_2 distribution surrounding roads and its titration effect on O_3. SF values are generally higher in autumn than other seasons, which corresponds to the O_3 formation peak in Hong Kong and its surrounding regions [53].

The current FSM network represents the combined health risks (%AR_{total}) well, which is the sum of %AR for all selected pollutants. Almost all land areas are represented with an SF > 0.9, with small exceptions of tunnel exits (Fig 7). This is due to the additive nature of %AR (Eq 5: Population-health network representation index). In Hong Kong, short-term hospital admission risk (%AR_{total}) is highly dominated by NO_2 and O_3 (Table 3), which together accounts for approximately 85% to 90% of all short-term hospital admission risks of air-pollution. Although %AR of NO_2 and O_3 exhibited substantial variations among FSMs, however, the added health risks are almost homogeneous as listed in Table 3, indicating the homogeneity of oxidative capacity (O_x) of air pollution throughout the whole domain. Under the influence of sunlight, NO_2 and O_3 are chemically converted by a series of reactions without net loss of their combined oxidative capacity [54]. The chemical interplay between NO_2 and O_3 leads to anti-correlated patterns for both pollutants [55], but keeps %AR_{total} values largely constant in space. Due to these effects, the FSM network is achieving good representativeness of %AR_{total} for both annual and seasons.

Population-based health risk representativeness

The aggregate population under well-represented (SF> 0.9) area was 2.7 million, 1.6 million, 1.0 million, and 0.5 million for PM_{10}, $PM_{2.5}$, O_3, NO_2, respectively, which account for 38%, 23%, 14% and 8% of the total population. The population-based health risk representativeness presents quite different patterns among FSMs compared to the area-based representativeness, as shown in Fig 8. For example, the SP station presents the largest well-represented population for PM, but it only ranks the 6th and 7th in representing areas for $PM_{2.5}$ and PM_{10}, respectively. The background station has the largest well-represented areas for all selected pollutants, but least well-represented population among all FSMs. The discrepancies in the ranking between area-based and population-based representativeness reflect the heterogeneity of population distribution. For example, the SP station is located at a densely populated district with average population density of over 40,000 persons/km^2 while the background station is located on a rural island which barely have no inhabitants.

The relationship between area-based and population-based representativeness is further evaluated using person correlation coefficients. Among the 16 FSMs, the correlations between these two methods are low (r < 0.3) and insignificant for all selected pollutants. Considering that MB station is a background station, which has quite a unique purpose and function than other stations, we re-conducted the correlation analysis by excluding the MB station. Among the 12 general and 3 roadside stations (n = 15), the correlation between well-represented area and well-represented population becomes significant only for NO_2 (r = 0.86), and remains insignificant for other pollutants. This indicates that the conventional evaluation methods, which are solely based on area is inadequate to address the representativeness of FSMs for public health, especially in the context of high population heterogeneity in urban areas. Although a high correlation is observed for NO_2, the overall well-represented population is small, less than 10% of the population.

The entire population (99.9%) is well-represented (SF > 0.9) by the FSMs for the combined health risks %AR_{total}. The correlation between well-represented area and well-represented population is high and significant (r = 0.94, p < 0.01). There is a large overlap between FSMs in their well-represented area or population for %AR_{total}, which makes it less sensitive to the heterogeneity in the population.

(a) Annual representativeness for Hong Kong (left) and its inset area (right)

(b) Spring

(c) Summer

(d) Autumn

(e) Winter

SF · FSM type • Background ▲ General ■ Roadside
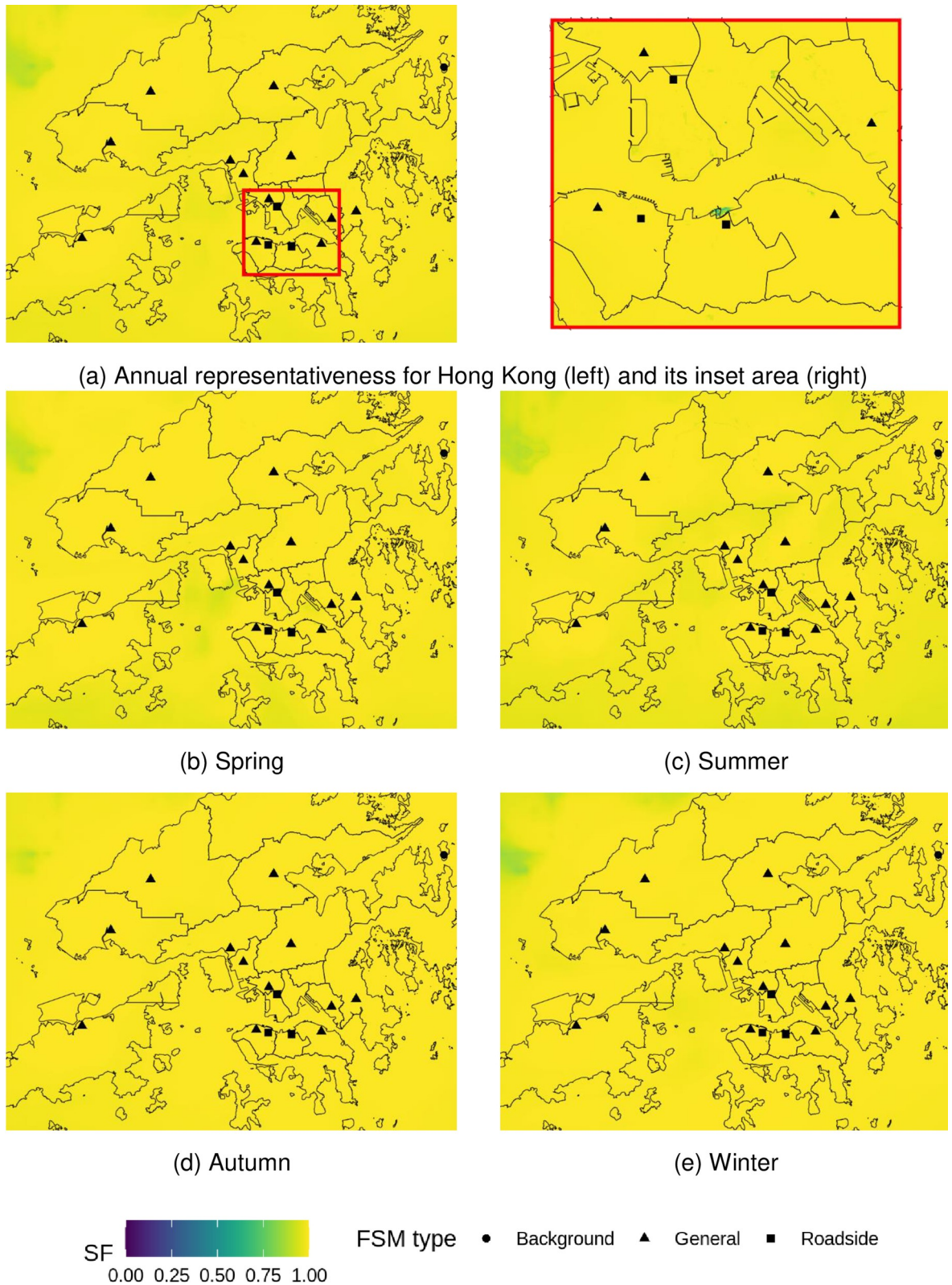0.00 0.25 0.50 0.75 1.00

Fig 7. Representativeness of total hospital admission risks (%AR total) from fixed site monitor (FSM) network over Hong Kong in 2019. Outlines of Hong Kong's districts reprinted from Esri China (Hong Kong) under a CC BY license, with permission from Esri China (Hong Kong), original copyright 2017.

https://doi.org/10.1371/journal.pone.0252290.g007

Table 3. Annual average %AR$_{total}$ at the location of each FSM (pseudo-station), and its contribution from different pollutants.

Station	Station Type	%AR$_{total}$	Contribution from each pollutant (in %)		
			PM	NO$_2$	O$_3$
MB	Background	5.8	10.7	9.3	80.0
CB	Roadside	6.4	15.2	44.5	40.3
CL	Roadside	7.1	17.2	56.6	26.2
MK	Roadside	6.9	16.7	55.1	28.2
CW	General	6.0	13.4	38.1	48.4
EN	General	5.8	11.6	19.9	68.5
KC	General	5.9	12.9	42.6	44.5
KT	General	6.3	14.5	39.0	46.6
ST	General	5.9	12.6	34.7	52.7
SP	General	6.0	13.7	43.0	43.3
TP	General	6.0	12.1	26.9	61.0
TK	General	5.9	12.2	22.2	65.7
TW	General	5.9	12.7	39.9	47.4
TM	General	5.9	12.0	33.7	54.3
TC	General	5.8	10.7	19.4	69.9
YL	General	5.9	12.1	30.4	57.5

https://doi.org/10.1371/journal.pone.0252290.t003

Annual and seasonal PHNI

The annual and seasonal PHNI over the entire domain is presented in Table 4 for individual and combined %AR. The PHNI provides an overall evaluation of the representativeness of the FSM network for public health, with values from 0 to 1 representing bad to good quality.

Amongst the four pollutants, the FSM network is best able to represent the population's health risks for PM, with annual PHNI of 0.87 for PM$_{10}$ and 0.82 for PM$_{2.5}$, respectively. Inter-seasonal variation in PHNI is 0.14 (0.77–0.91) for PM$_{2.5}$ and 0.1 (0.83–0.93) for PM$_{10}$, with the highest PHNI found in winter for both PM, indicating a strong regional impacts on public health risks to PM in Hong Kong.

The annual PHNI for NO$_2$ is 0.59, which is lower compared to PM. This is major due to the heterogeneity of NO$_2$ distributions over Hong Kong which is related to traffic emissions and urban morphology such as street canyons [10]. The inter-season variations in PHNI are relatively small, ranging from 0.59 in spring to 0.65 in winter (Table 4). Under the Asian monsoon system, the air plume in Hong Kong shifts from the south in summer, which will bring fresh ocean air, to North in winter, which will bring continental air pollution from Pearl River Delta region. However, the PHNI for NO$_2$ is quite similar between summer (0.63) and winter (0.65), indicating that NO$_2$ pollution in Hong Kong is more related to local sources.

The annual PHNI for O$_3$ is considerably higher compared to NO$_2$, with an annual average of PHNI of 0.78. The PHNI for O$_3$ is much higher in autumn (0.87) than other seasons (0.77–0.79), which is related to increase contribution from regional pollution and increased photo-chemistry under sunlight in autumn.

The PHNI for %AR$_{total}$ is nearly 1 for both annual and seasonal scales, indicating the current FSM network has a good capacity to represent short-term public health risks to air pollution in Hong Kong. As mentioned before, the short-term risks (%AR$_{total}$) is dominated by %AR NO$_2$ and %AR O$_3$, which are anti-correlated in the study domain. The homogeneity nature of the %AR$_{total}$ makes it less sensitive to the location of FSMs and heterogeneity of the population.
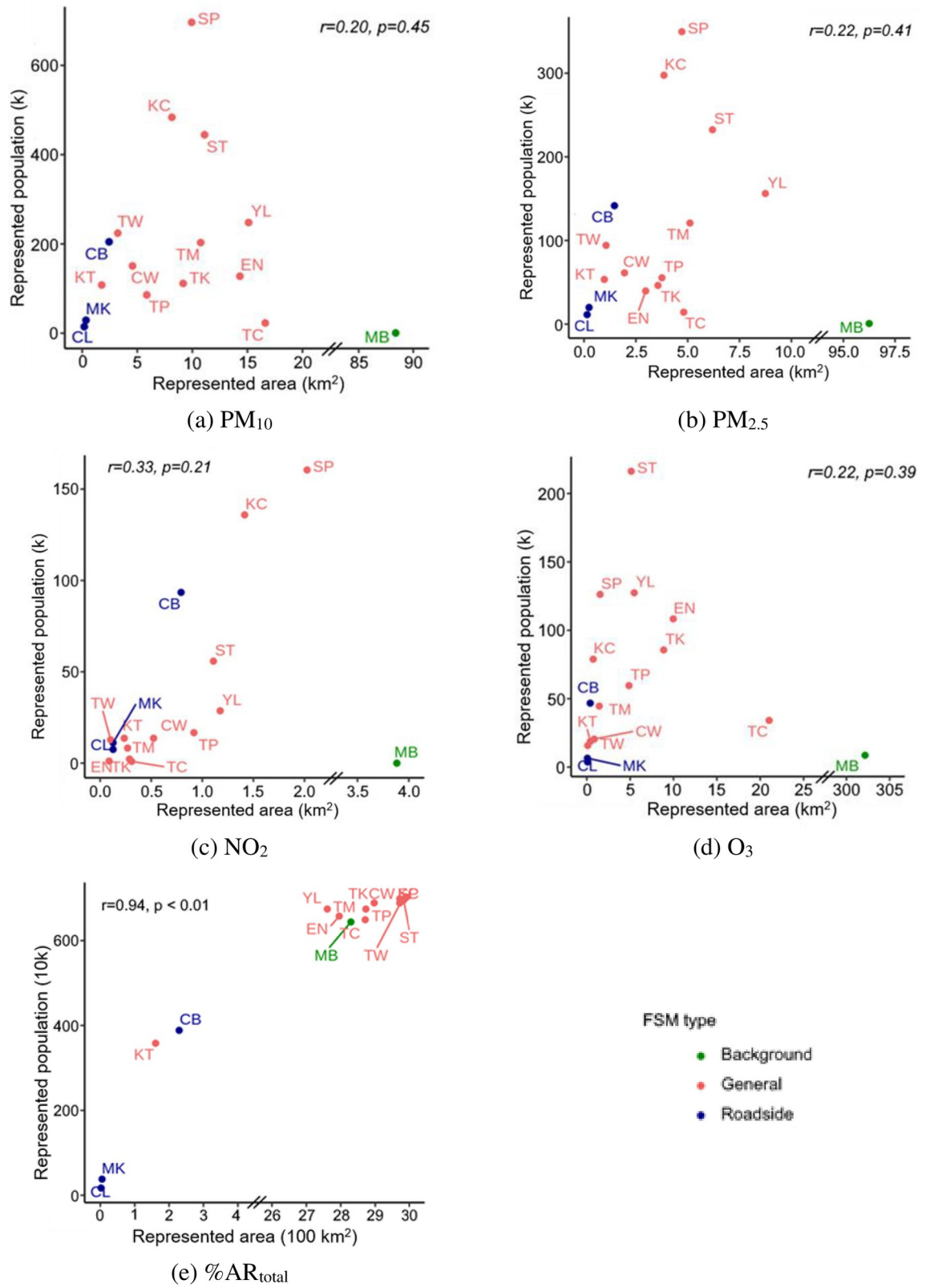
(a) PM$_{10}$

(b) PM$_{2.5}$

(c) NO$_2$

(d) O$_3$

(e) %AR$_{total}$

Fig 8. Represented area and represented population (SF > 0.9) by fixed site monitor (FSM).

https://doi.org/10.1371/journal.pone.0252290.g008

Table 4. Annual and seasonal health-based index of representation quality (PHNI) of the FSM network.

Base pollutant	Annual	Spring	Summer	Autumn	Winter
%AR$_{PM10}$	0.87	0.84	0.83	0.93	0.93
%AR$_{PM2.5}$	0.82	0.79	0.77	0.92	0.91
%AR$_{NO2}$	0.59	0.59	0.63	0.60	0.65
%AR$_{O3}$	0.78	0.77	0.77	0.87	0.79
%AR$_{total}$	1.00	1.00	1.00	1.00	1.00

https://doi.org/10.1371/journal.pone.0252290.t004

PHNI comparison among districts

Hong Kong's territory is divided into 18 administrative districts. Smaller districts are located in the densely populated city centre, and larger districts are predominantly located in the outlying and more rural areas. Annual PHNI was calculated for each district and %AR, as seen in Fig 9.

The district-level PHNI values ranged from 0.74 to 0.9 for PM$_{2.5}$ and from 0.78 to 0.92 for PM$_{10}$. Higher PHNI values were found in inner districts surrounding city centre, such as Sham Shui Po, and lower PHNI values were found in outlying districts such as North and Southern districts. The allocations of existing FSMs are sparser in remote areas than city centres, making it more challenging to reflect the public health risks given the heterogeneity in pollution and population.

The district-level PHNI values ranged from 0.34 to 0.81 for NO$_2$. Higher PHNIs are highly concentrated in districts where roadside stations are located. As discussed in previous sections, NO$_2$ pollution is closely related to traffic emission. Roadside stations are situated in busy traffic roads with sampling inlet much closer to the ground than general and background sites, which make them more appropriate to reflect public health risks to NO$_2$ in their located districts.

(a) PM$_{10}$ (b) PM$_{2.5}$ (c) NO$_2$
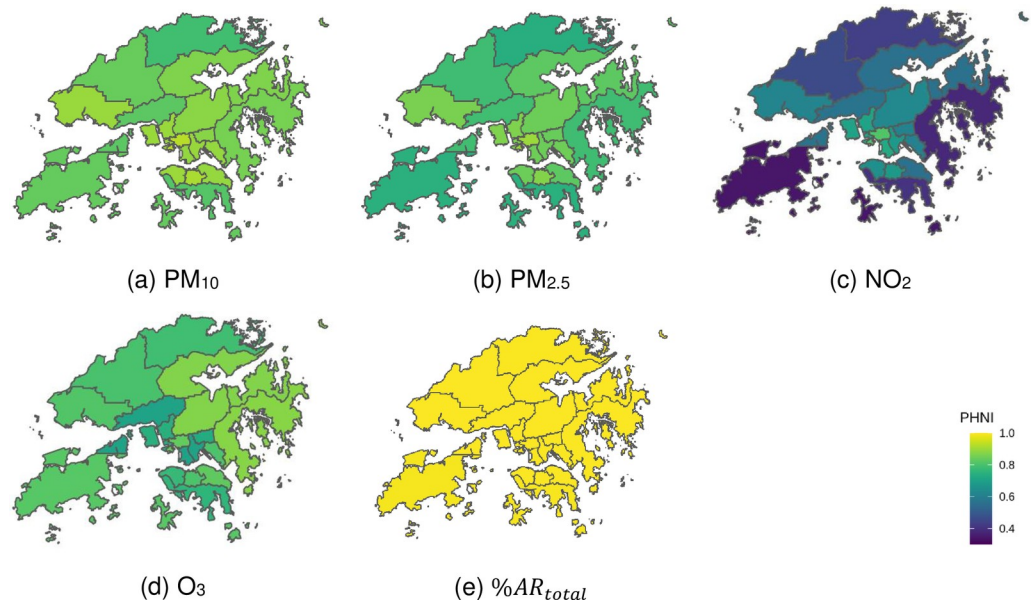
(d) O$_3$ (e) %AR$_{total}$

Fig 9. District-level population-based health representativeness for Hong Kong. Outlines of Hong Kong's districts reprinted from Esri China (Hong Kong) under a CC BY license, with permission from Esri China (Hong Kong), original copyright 2017.

https://doi.org/10.1371/journal.pone.0252290.g009

The district-level PHNI ranged from 0.71 to 0.88 for O_3. Higher PHNIs are found in districts near the background station, indicating impacts of background or regional O_3 pollution on public health risk.

Hospital admission risks of all pollutants combined (%AR_{total}) are well-represented by the current sensor network in all districts (PNHI > 0.99), resulting in a uniform high representation that contrasts the variations found for individual pollutants (Fig 9).

Discussion

This proposed population-based representation evaluation method is different from existing methods that rely on spatial concentrations [19, 21, 56]. Based on our results, there is no apparent correlation between the size of the represented area and the actually represented population among the FSMs for any of the selected pollutants. Therefore, it cannot be taken for granted that an FSM network successful in spatially representing an urban area is also successful in conveying its population. The proposed population-health based metric integrates population distribution and risk factors with spatial pollutant concentrations in evaluating the representativeness quality of an FSM network, which can better address the concerns on public health risks to air pollution.

Compared to concentration representativeness based on single pollutants, a major advantage of health-based representativeness is its ability to combine the health risks of various pollutants into a single metric (Eq 5). We found high %AR_{total} representation throughout the whole study area. These results indicate that the current FSM network in Hong Kong can reflect the combined effects of air pollution on short-term health risks well. Nevertheless, it should be noted that the short term %AR_{total} is more uniformly distributed in Hong Kong due to the dominance and anti-correlation between NO_2 and O_3 under the VOC-limited regime. The homogeneity nature of %AR_{total} may not hold in other places and thus it should not be taken for granted that the FSM network will always reflect well the combined effects.

The proposed PHNI index is not only useful to evaluate the quality of an existing FSM network but also can help improve the network during design or in operation. A network with much overlap is unnecessarily expensive, and a cost-effective solution always aims at reducing station overlap [21, 57]. An optimization effort aimed at maximising PHNI removes the problem of overlap, as it is aimed at optimizing multi-pollutant based %AR_{total}, with only the best representation by any FSM station of a given cell counting into the metric (Eq 6). Therefore, the decision of whether and where to add or remove an FSM sensor should always be driven from a holistic network-perspective in the interface of existing stations, population exposure and the health effects of the pollutant.

The %AR for each individual pollutant is also important for provide health risk information. Some subgroups of the population are especially vulnerable a single pollutant, e.g. through an allergic pathway [58, 59]. For these groups, the representation of a specific pollutant is critical. Besides, current metrics are not integrating long-term health risks due to the lack of health-coefficients. Pollutants such as $PM_{2.5}$ and PM_{10} heavily affects long-term health. Thus, the representativeness evaluation of PM may serve as an indicator of long-term health risks. Another critical step is to enable the public to identify their best-representing FSM station by more than rough guidance based on administrative boundaries or proximity to the next station [35]. We suggest more research into effective and empowering use of FSM network data.

The representativeness of current FSM in Hong Kong is still challenging for individual pollutants, especially for local pollutants such as NO_2. The majority of stations represent less than 1 km^2 area for NO_2. This is in line with previous findings from general stations in the city-

centre of Paris [19]. Our results further show that most of the stations well represents less than 20,000 people. Apart from the sometimes suggested [60], but in reality arguably difficult reallocation of sensors, smart city infrastructure opens a promising avenue to increase representation of the population [61]. For example, low-cost sensors can be deployed at a multitude of locations with a relatively cheap price tag for set-up and maintenance. However, such sensors suffer from issues of drift, interference and low lifetime [9]. An integration of smart-city infrastructure into existing FSM networks is thus a challenging task. Here, the proposed network index can consider both traditional and new approaches towards measuring air quality. A higher score of the network index can be achieved both by adding high-grade traditional sensors (limited to few locations, but with a high measurement quality) and low-cost sensors (at many locations, but with more observation error). The observation error of low-cost sensors as sensor drift [62] can be accommodated by the addition of an error-term during SF-calculation. Further research is warranted to show the cost-effectiveness of both approaches, as well as their optimal locations based on an optimization for population-health representativeness.

As global cities are increasingly interwoven, data driven [63] and in competition, managing environmental pollution becomes an essential criterion for the success of a city [27]. Here, due to its grounding in health and population, the proposed metrics make management infrastructures of environmental pollution (FSM networks) comparable between cities of different sizes and characteristics. Thus, it would be of great interest to expand the proposed methodology to several of cities, consequently enabling the addition of FSM network quality as a factor of sustainability indices and city rankings.

Conclusions

Existing methodologies judge the representativeness of urban air quality monitoring networks by spatial representativeness of a single pollutant. This paper demonstrates shortcomings of this approach. Firstly, the representativeness of multiple pollutants cannot be combined into a single metric. Secondly, we show that in Hong Kong, spatial representatives areas sizes are not correlated with actual represented population ($p > 0.05$ for all pollutants, n = 16). To overcome these challenges, we derived a health -and population-based metric (PHNI) for the representativeness of urban air quality monitoring networks. By basing the metric not on represented pollution concentration, but on represented additive short-term health impacts of the pollutants (%AR), an overarching %AR_{total} can be calculated. Results show that in our study area, representativeness values varied with pollutants, with regionally influenced PM better represented ($PHNI_{PM10} = 0.87$, $PHNI_{PM2.5} = 0.82$) than more locally gaseous pollutants ($PHNI_{NO2} = 0.59$, $PHNI_{O3} = 0.78$). Due to the dominance of these gaseous pollutants on %AR_{total} as well as their anticorrelated chemical interplay in Hong Kong's VOC-limited regime, total short-term health effects of the large majority of the population (99.9% of 7.5 million residents) was found to be well represented by the current sensor network (SF > 0.9). In contrast to that, the well-represented population was 2.7 million, 1.6 million, 1.0 million, and 0.5 million for PM_{10}, $PM_{2.5}$, O_3, NO_2, respectively. District-level difference in representation quality were especially large for NO_2, with rural districts being less-well represented than urban districts. We explain this by the relative abundance of monitors in smaller, urban districts and dedicated roadside stations capturing spatially and temporally varying traffic emissions. The adoption of a population-health based framework makes monitoring efforts comparable and can lead to improved inter-city competition for sustainable development.

Author Contributions

Conceptualization: Wenwei Che.

Data curation: Jimmy C. H. Fung.

Formal analysis: Tilman Leo Hohenberger.

Funding acquisition: Wenwei Che, Alexis K. H. Lau.

Investigation: Tilman Leo Hohenberger, Wenwei Che, Jimmy C. H. Fung.

Methodology: Tilman Leo Hohenberger.

Resources: Alexis K. H. Lau.

Supervision: Wenwei Che, Alexis K. H. Lau.

Visualization: Tilman Leo Hohenberger.

Writing – original draft: Tilman Leo Hohenberger.

Writing – review & editing: Wenwei Che.

References

1. D'amato G, Cecchi L, Amato D', Liccardi G. Urban Air Pollution and Climate Change as Environmental Risk Factors of Respiratory Allergy: An Update. J Investig Allergol Clin Immunol. 2010. PMID: 20461963

2. Sunyer J. Urban air pollution and chronic obstructive pulmonary disease: a review Histological background. Eur Respir J. 2001; 17.

3. Nyberg F, Järup L, Bellander T, Berglind N, Jakobsson R, Pershagen G. Urban Air Pollution and Lung Cancer in Stockholm. Source Epidemiol. 2000. https://doi.org/10.1097/00001648-200009000-00002 PMID: 10955399

4. Bhatnagar A. Environmental cardiology: Studying mechanistic links between pollution and heart disease. Circulation Research. 2006. pp. 692–705. https://doi.org/10.1161/01.RES.0000243586.99701.cf PMID: 17008598

5. World Health Organization. Ambient Air Pollution: A global assessment of exposure and burden of disease. World Heal Organ. 2016.

6. Manisalidis I, Stavropoulou E, Stavropoulos A, Bezirtzoglou E. Environmental and Health Impacts of Air Pollution: A Review. Frontiers in Public Health. Frontiers Media S.A.; 2020. https://doi.org/10.3389/fpubh.2020.00014 PMID: 32154200

7. Mustafić H, Jabre P, Caussin C, Murad MH, Escolano S, Tafflet M, et al. Main air pollutants and myocardial infarction: A systematic review and meta-analysis. JAMA—J Am Med Assoc. 2012; 307: 713–721. https://doi.org/10.1001/jama.2012.126 PMID: 22337682

8. Duyzer J, van den Hout D, Zandveld P, van Ratingen S. Representativeness of air quality monitoring networks. Atmos Environ. 2015; 104: 88–101. https://doi.org/10.1016/j.atmosenv.2014.12.067

9. Snyder EG, Watkins TH, Solomon PA, Thoma ED, Williams RW, Hagler GSW, et al. The changing paradigm of air pollution monitoring. Environ Sci Technol. 2013; 47: 11369–11377. https://doi.org/10.1021/es4022602 PMID: 23980922

10. Che W, Frey HC, Fung JCH, Ning Z, Qu H, Lo HK, et al. PRAISE-HK: A personalized real-time air quality informatics system for citizen participation in exposure and health risk management. Sustain Cities Soc. 2020; 54. https://doi.org/10.1016/j.scs.2019.101935 PMID: 32288992

11. Li T, Zhou XC, Ikhumhen HO, Difei A. Research on the optimization of air quality monitoring station layout based on spatial grid statistical analysis method. Environ Technol (United Kingdom). 2018; 39: 1271–1283. https://doi.org/10.1080/09593330.2017.1327557 PMID: 28475472

12. Righini G, Cappelletti A, Ciucci A, Cremona G, Piersanti A, Vitali L, et al. GIS based assessment of the spatial representativeness of air quality monitoring stations using pollutant emissions data. Atmos Environ. 2014; 97: 121–129. https://doi.org/10.1016/j.atmosenv.2014.08.015

13. Janssen S, Dumont G, Fierens F, Deutsch F, Maiheu B, Celis D, et al. Land use to characterize spatial representativeness of air quality monitoring stations and its relevance for model validation. Atmos Environ. 2012; 59: 492–500. https://doi.org/10.1016/j.atmosenv.2012.05.028

14. Yu T, Wang W, Ciren P, Sun R. An assessment of air-quality monitoring station locations based on satellite observations. Int J Remote Sens. 2018; 39: 6463–6478. https://doi.org/10.1080/01431161.2018.1460505

15. Piersanti A, Vitali L, Righini G, Cremona G, Ciancarella L. Spatial representativeness of air quality monitoring stations: A grid model based approach. Atmos Pollut Res. 2015; 6: 953–960. https://doi.org/10.1016/j.apr.2015.04.005

16. Vitali L, Morabito A, Adani M, Assennato G, Ciancarella L, Cremona G, et al. A Lagrangian modelling approach to assess the representativeness area of an industrial air quality monitoring station. Atmos Pollut Res. 2016; 7: 990–1003. https://doi.org/10.1016/j.apr.2016.06.002

17. Rivas E, Santiago JL, Lechón Y, Martín F, Ariño A, Pons JJ, et al. CFD modelling of air quality in Pamplona City (Spain): Assessment, stations spatial representativeness and health impacts valuation. Sci Total Environ. 2019; 649: 1362–1380. https://doi.org/10.1016/j.scitotenv.2018.08.315 PMID: 30308906

18. Aikawa M, Hiraki T, Eiho J. Grouping and representativeness of monitoring stations based on wind speed and wind direction data in urban areas of Japan. Environmental Monitoring and Assessment. 2008. pp. 411–418. https://doi.org/10.1007/s10661-007-9696-0 PMID: 17610033

19. Rodriguez D, Valari M, Payan S, Eymard L. On the spatial representativeness of NOX and PM10 monitoring-sites in Paris, France. Atmos Environ X. 2019; 1. https://doi.org/10.1016/j.aeaoa.2019.100010

20. European Commission. Directive 2008/50/EC of the European Parliament and of the Council of 21 May 2008 on ambient air quality and cleaner air for Europe. 2008 pp. 1–44.

21. Hao Y, Xie S. Optimal redistribution of an urban air quality monitoring network using atmospheric dispersion model and genetic algorithm. Atmos Environ. 2018; 177: 222–233. https://doi.org/10.1016/j.atmosenv.2018.01.011

22. Wong TW, Tam WWS, Yu ITS, Lau AKH, Pang SW, Wong AHS. Developing a risk-based air quality health index. Atmos Environ. 2013; 76: 52–58. https://doi.org/10.1016/j.atmosenv.2012.06.071

23. Stieb DM, Burnett RT, Smith-Doiron M, Brion O, Hwashin HS, Economou V. A new multipollutant, no-threshold air quality health index based on short-term associations observed in daily time-series analyses. J Air Waste Manag Assoc. 2008; 58: 435–450. https://doi.org/10.3155/1047-3289.58.3.435 PMID: 18376646

24. Kousa A, Kukkonen J, Karppinen A, Aivi Aarnio P, Koskentalo T. A model for evaluating the population exposure to ambient air pollution in an urban area. Atmos Environ. 2002.

25. Gan WQ, McLean K, Brauer M, Chiarello SA, Davies HW. Modeling population exposure to community noise and air pollution in a large metropolitan area. Environ Res. 2012; 116: 11–16. https://doi.org/10.1016/j.envres.2012.04.001 PMID: 22520824

26. Douglass M. From global intercity competition to cooperation for livable cities and economic resilience in Pacific Asia. Environ Urban. 2002; 14: 53–68. https://doi.org/10.1177/095624780201400105

27. Giffinger R, Haindlmaier G, Kramar H. The role of rankings in growing city competition. Urban Res Pract. 2010; 3: 299–312. https://doi.org/10.1080/17535069.2010.524420

28. Acuto M, Rayner S. City networks: Breaking gridlocks or forging (new) lock-ins? Int Aff. 2016; 92: 1147–1166. https://doi.org/10.1111/1468-2346.12700

29. Berry BJL. Urbanization. Urban Ecol. 2008; 25–48.

30. Yang K, Teng M, Luo Y, Zhou X, Zhang M, Sun W, et al. Human activities and the natural environment have induced changes in the PM2.5 concentrations in Yunnan Province, China, over the past 19 years. Environ Pollut. 2020; 265. https://doi.org/10.1016/j.envpol.2020.114878 PMID: 32806442

31. Yang K, Shi Y, Luo Y, Liu R, Sun W, Sun M. Assessing spatiotemporal air environment degradation and improvement represented by PM2.5 in China using two-phase hybrid model. Sustain Cities Soc. 2020; 59. https://doi.org/10.1016/j.scs.2020.102180

32. Hong Kong Planning Department. Land Utilization in Hong Kong 2018. 2018. Available: https://www.pland.gov.hk/pland_en/info_serv/statistic/landu.html

33. Hong Kong Census and Statistics Department. Hong Kong Statistics. 2020. Available: https://www.censtatd.gov.hk/hkstat/sub/bbs.jsp

34. Louie PKK, Watson JG, Chow JC, Chen A, Sin DWM, Lau AKH. Seasonal characteristics and regional transport of PM2.5 in Hong Kong. Atmos Environ. 2005; 39: 1695–1710. https://doi.org/10.1016/j.atmosenv.2004.11.017

35. Hong Kong EPD. Air Quality Monitoring Stations. 2020. Available: https://www.aqhi.gov.hk/en/monitoring-network/air-quality-monitoring-stations.html https://doi.org/10.1016/j.ejmg.2020.104062 PMID: 32931946

36. Binkowski FS, Roselle SJ. Models-3 Community Multiscale Air Quality (CMAQ) model aerosol component 1. Model description. J Geophys Res Atmos. 2003; 108.

37. McHugh CA, Carruthers DJ, Edmunds HA. ADMS-Urban: An air quality management system for traffic, domestic and industrial pollution. Int J Environ Pollut. 1997. https://doi.org/10.1504/IJEP.1997.028218

38. Powers JG, Klemp JB, Skamarock WC, Davis CA, Dudhia J, Gill DO, et al. The weather research and forecasting model. Bull Am Meteorol Soc. 2017. https://doi.org/10.1175/BAMS-D-15-00308.1

39. Houyoux MR, Vukovich JM. Updates to the Sparse Matrix Operator Kernel Emissions (SMOKE) modeling system and integration with Models-3. Proc Emiss Invent Reg Strateg Futur. 1999.

40. Beevers SD, Kitwiroon N, Williams ML, Kelly FJ, Ross Anderson H, Carslaw DC. Air pollution dispersion models for human exposure predictions in London. J Expo Sci Environ Epidemiol. 2013; 23: 647–653. https://doi.org/10.1038/jes.2013.6 PMID: 23443237

41. Willmott CJ. On the validation of models. Phys Geogr. 1981; 2: 184–194. https://doi.org/10.1080/02723646.1981.10642213

42. Kang D, Mathur R, Rao ST, Yu S. Bias adjustment techniques for improving ozone air quality forecasts. J Geophys Res Atmos. 2008; 113: 1–17. https://doi.org/10.1029/2008JD010151

43. Wai WT, San WTW, Shun MAWH, Hon ALK, Ng MSKW, Yeung MD, et al. A study of the air pollution index reporting system. Stat Modelling. 2012; 13: 15.

44. Nappo CJ. The workshop on the representativeness of meteorological observations (Boulder). Bull Am Meteorol Soc. 1982.

45. Dobson JE, Bright EA, Coleman PR, Durfee RC, Worley BA. LandScan: A global population database for estimating populations at risk. Photogramm Eng Remote Sensing. 2000; 66: 849–857.

46. Lin C, Li Y, Lau AKH, Deng X, Tse TKT, Fung JCH, et al. Estimation of long-term population exposure to PM2.5 for dense urban areas using 1-km MODIS data. Remote Sens Environ. 2016; 179: 13–22. https://doi.org/10.1016/j.rse.2016.03.023

47. Hong Kong Census and Statistics Department. 2011 Population Census—Summary results. 2012. Available: https://www.census2011.gov.hk/pdf/summary-results.pdf

48. Hijmans RJ. Package 'raster'—Geographic Data Analysis and Modeling. CRAN Repository. 2019. Available: https://cran.r-project.org/package=raster

49. Sillman S. Chapter 12 The relation between ozone, NOx and hydrocarbons in urban and polluted rural environments. Dev Environ Sci. 2002; 1: 339–385. https://doi.org/10.1016/S1474-8177(02)80015-8

50. Ghazali NA, Ramli NA, Yahaya AS, Yusof NFFM, Sansuddin N, Al Madhoun WA. Transformation of nitrogen dioxide into ozone and prediction of ozone concentrations using multiple linear regression techniques. Environ Monit Assess. 2010; 165: 475–489. https://doi.org/10.1007/s10661-009-0960-3 PMID: 19440846

51. Huang XHH, Bian Q, Ng WM, Louie PKK, Yu JZ. Characterization of PM2.5 major components and source investigation in suburban Hong Kong: A one year monitoring study. Aerosol Air Qual Res. 2014; 14: 237–250. https://doi.org/10.4209/aaqr.2013.01.0020

52. Yuan Z, Lau AKH, Zhang H, Yu JZ, Louie PKK, Fung JCH. Identification and spatiotemporal variations of dominant PM10 sources over Hong Kong. Atmos Environ. 2006; 40: 1803–1815. https://doi.org/10.1016/j.atmosenv.2005.11.030

53. Placet M, Mann CO, Gilbert RO, Niefer MJ. Emissions of ozone precursors from stationary sources: A critical review. Atmos Environ. 2000; 34: 2183–2204. https://doi.org/10.1016/S1352-2310(99)00464-1

54. Han S, Bian H, Feng Y, Liu A, Li X, Zeng F, et al. Analysis of the relationship between O3, NO and NO2 in Tianjin, China. Aerosol Air Qual Res. 2011; 11: 128–139. https://doi.org/10.4209/aaqr.2010.07.0055

55. Wang Y, Wang H, Guo H, Lyu X, Cheng H, Ling Z, et al. Long-term O3-precursor relationships in Hong Kong: Field observation and model simulation. Atmos Chem Phys. 2017; 17: 10919–10935. https://doi.org/10.5194/acp-17-10919-2017

56. Mocerino L, Murena F, Quaranta F, Toscano D. A methodology for the design of an effective air quality monitoring network in port areas. Sci Rep. 2020; 10. https://doi.org/10.1038/s41598-019-57244-7 PMID: 31941929

57. Martin F, Fileni L, Palomino I, Vivanco MG, Garrido JL. Analysis of the spatial representativeness of rural background monitoring stations in Spain. Atmos Pollut Res. 2014; 5: 779–788. https://doi.org/10.5094/APR.2014.087

58. Van Der Vliet A. Nox enzymes in allergic airway inflammation. Biochim Biophys Acta—Gen Subj. 2011; 1810: 1035–1044. https://doi.org/10.1016/j.bbagen.2011.03.004 PMID: 21397663

59. Baldacci S, Maio S, Cerrai S, Sarno G, Baïz N, Simoni M, et al. Allergy and asthma: Effects of the exposure to particulate matter and biological allergens. Respir Med. 2015; 109: 1089–1104. https://doi.org/10.1016/j.rmed.2015.05.017 PMID: 26073963

60. Li J, Zhang H, Luo Y, Deng X, Grieneisen ML, Yang F, et al. Stepwise genetic algorithm for adaptive management: Application to air quality monitoring network optimization. Atmos Environ. 2019; 215. https://doi.org/10.1016/j.atmosenv.2019.116894

61. Postolache OA, Dias Pereira JM, Silva Girão PMB. Smart sensors network for air quality monitoring applications. IEEE Trans Instrum Meas. 2009; 58: 3253–3262. https://doi.org/10.1109/TIM.2009.2022372

62. Hagan DH, Isaacman-Vanwertz G, Franklin JP, Wallace LMM, Kocar BD, Heald CL, et al. Calibration and assessment of electrochemical air quality sensors by co-location with regulatory-grade instruments. Atmos Meas Tech. 2018; 11: 315–328. https://doi.org/10.5194/amt-11-315-2018

63. Bibri SE, Krogstie J. Smart sustainable cities of the future: An extensive interdisciplinary literature review. Sustainable Cities and Society. Elsevier Ltd; 2017. pp. 183–212. https://doi.org/10.1016/j.scs.2017.02.016